IET Electric Power Applications

ORIGINAL RESEARCH

Genetic algorithm-based approach for torque control and increased efficiency across an optimised speed range in switched reluctance drives

Euan MacRae[1] | Ali Abdel-Aziz[1] | Khaled Ahmed[1] | Richard Pollock[2] | Barry W. Williams[1]

[1]Department of Electronic and Electrical Engineering, University of Strathclyde, Glasgow, Scotland, UK

[2]Technelec.ltd, Oakham, UK

Correspondence

Euan MacRae, Department of Electronic and Electrical Engineering, University of Strathclyde, Glasgow, Scotland, UK.
Email: euan.macrae@strath.ac.uk

Abstract

This paper presents a novel genetic algorithm (GA) design for current profiling in switched reluctance machines that eliminates torque ripple (TR) while inherently guaranteeing minimal RMS currents across the machines speed range. Minimising RMS current provides an increase to machine efficiency and the elimination of TR is required for potential SRM applications such as traction vehicles. This paper proposes a novel method for intentional greater-than-two-phase overlap in the algorithm design. This allows any SRM configuration capable of three or more phase conduction to utilise its full speed range with zero torque ripple, in the case where it is limited using two-phase torque sharing. An optimal set of current profiles is created using the algorithm across the full speed range of an exemplary 8/6 SRM and these are analysed. A current profiling-based control scheme using these results is then proposed and simulated for the 8/6 SRM. This is then compared to classical and recently published SRM control methods to highlight the merits of the overall GA design and its resultant control scheme.

1 | INTRODUCTION

In recent times, the switched reluctance machine (SRM) has received attention as a candidate topology for applications such as electric vehicles (EVs) [1, 2]. This is due to its offering a host of attractive characteristics which lend themselves to the challenges of EV operation. From an environmental perspective, the SRM contains no rare earth permanent magnet materials and is typically composed of silicon steel and copper. This leads to a low-cost, robust design which provides a strong fault tolerance and broad speed range [3, 4]. The SRM like any electrical machine design has its drawbacks. These being primarily non-linear magnetic characteristics and tendency to generate unnecessary acoustic noise, where both are products of the SRMs doubly salient stator and rotor design. In general, these makes the machine difficult to operate without a control

strategy specific to the topology [5], given that each phase operates with discrete torque production. This torque production coupled with non-linear magnetic characteristics give rise to the torque ripple (TR) that the machine is associated with, where it can become significant at phase commutation without bespoke control. For the SRM to be an alternative to machine designs used in commercial EVs such as the permanent magnet synchronous machine or induction machine, this TR must be eliminated, its efficiency must also be optimised, and torque overall control linearised across the machines base speed range.

TR reduction is an important research field within SRM control theory. Alternatives to control exist in terms of machine design by adjustment of the SRM's rotor/stator shapes or pole ratio [5–9]. These provide TR reduction, but changes to the machine can never truly eliminate TR as there will be always some form of phase commutation if operating with

single phase torque production. Comparatively, control schemes can eliminate TR and are in general cheaper and simpler to implement on a given SRM than a change in structure [6]. Control of torque in the SRM exists primarily under two families: direct control and indirect control.

Direct torque control (DTC) was first proposed in ref. [9]. It utilises a lookup table (LUT) relating torque T, current I, and rotor angle θ $(T - I - \theta)$, to estimate torque. A vector for rate of change of stator flux is then used to indicate the flux and conduction, which is then regulated by a hysteresis current band controller. It offers reduced in TR but requires variable switching frequency. Machine parameters are also required but with the availability of finite element analysis (FEA) software, this is not necessarily a difficulty. Similar to DTC, direct instantaneous torque control, ref. [10] proposes estimation of torque instantaneously as the name suggests, using terminal measurements. Torque is calculated using a LUT relating flux linkage λ, current, and rotor angle $(T - I - \lambda)$, where λ is found from terminal voltage and phase winding loss. It offers the same advantages as DTC, without a high-resolution encoder and is readily modifiable; such as the schemes presented in ref. [11] or ref. [12].

Indirect torque control schemes can be deployed using SRM variables which directly influence torque production. For example, in ref. [13] an offline method referred to now as 'current profiling' is proposed. It uses a LUT, storing predetermined single phase current profiles across the operational range of a 4ϕ SRM which in turn produce desired values of torque. It proposes the first offline use of the intentional sharing of torque between SRM phases and could be considered a torque sharing function (TSF) before their formal establishment in literature. TSFs themselves are a popular offline or online control solution in SRMs and have many different variations across literature [14–16]. As described before, they operate on some form of torque sharing at phase commutation between the outgoing and incoming phase. When this overlap occurs, there is a mathematical strategy deployed which will determine the distribution of torque between the phases to produce theoretically zero torque ripple (ZTR) while typically having some secondary objective such as reducing RMS current. An online example of indirect torque control is given in ref. [17], where the controlled variables are the turn-on and turn-off angles of the SRMs phases and each based upon different criteria. The turn-on angle is calculated based upon changes in machine speed and phase RMS current. The turn-off angle is calculated after this using the turn-on angle to introduce an optimal decay path for the current during phase commutation. This strategy provides a stable significant reduction in TR during operation but is limited in any manipulation of the current profiles it produces.

Given the volume and maturity of research in SRM control, completely new methods for TR reduction or elimination have become rarer. Instead focus has tended to shift towards improving existing techniques from novel perspectives, where optimisation techniques have contributed significantly in this regard. TSFs, for example, have been modified with online algorithm-based approaches such as using ant colony in ref. [18] or exhaustive search [19], optimising switching angles to extend speed range and minimise RMS

current. A DTC optimisation is proposed in ref. [20], which utilises a newer form of meta heuristic algorithm, the wolf and coyote. Using this approach, TR is reduced while also providing stable speed control as an alternative to using PI control. Current profiling has been carried out using an offline genetic algorithm (GA)-based optimisation approach in ref. [21]. It establishes the idea of calculating a theoretically minimal RMS current profile for any given SRM configuration as a benchmark for optimisation. It then uses this and two phase torque sharing in conjunction with the GA to produce optimally minimised RMS current profiles (1.16% above benchmark) with ZTR maintained. The main drawback of this method is that it only produces a partial speed range (72% at full load torque [FLT]) of a given 8/6 SRMs base speed due to the limitations of two-phase torque with the given DC link voltage V_{DC}. This is not necessarily true for any SRM configuration, but a robust optimisation method should operate the SRM across the full speed range.

Overall, this paper presents a novel method of SRM current profiling with a refined GA design, which utilises greater than two phases of simultaneous overlap with included variation in turn on and turn off angles. The idea of the intentional use of three phase overlap as an example is established, where instead of introducing a third phase that contributes TR unintentionally, the third phase is accounted for and used to operate the SRM at higher speeds while still maintaining ZTR. The GA uses an absolute minimal RMS current that is theoretical and obtained using the method in ref. [21]. The GA then uses this seeding to produce a range of optimal current profiles across the SRM full speed range which includes two phase overlap at low to mid speed range and three phase overlap in the upper speed range. These current profiles are then utilised in a proposed LUT-based linear control scheme.

The paper structure is as follows: Section 2 introduces the idea of operating an SRM across its full speed range with ZTR when two phase overlap limits this by introducing intentional greater than two phase overlap. Section 3 introduces the GA design to produce optimal current profiles while considering a given SRMs parameters, the available DC link voltage, and torque demand of operation. Section 4 validates the GA design using simulation results by producing optimal profiles using the GA across the speeds unattainable in ref. [21] using three phase overlap. A LUT based control scheme using the full speed range of profiles is then proposed and simulated. Finally, Section 5 compares the simulated control scheme to conventional SRM control for TR elimination and then compares to simulation results of advanced SRM control in recent publications. Table 1 presents the parameters of the 8/6 SRM used in this research study.

2 | TORQUE RIPPLE-FREE SPEED RANGE EXTENSION USING GREATER THAN TWO PHASE OVERLAP

Two phase torque sharing in principle allows successive SRM phases to overlap and conduct for a maximum angular period $\theta_{ov(2\phi)}$ (15° in this 8/6 case), determined using Equation (1),

which is established by TSFs using rotor pole pitch θ_r and stroke angle ε in Equation (2).

$$\theta_{\text{ov}(2\phi)} \leq \tfrac{1}{2}\theta_r - \varepsilon = \tfrac{1}{2} \times 60^\circ - 15^\circ = 15^\circ \quad (1)$$

$$\varepsilon = \frac{2\pi}{mN_r} = \frac{2\pi}{4 \times 6} = 15^\circ \quad (2)$$

This $\theta_{\text{ov}(2\phi)}$ can be realised at varied regions and angular lengths in θ_r but logically, will be wholly or majority in the positive torque production region to produce FLT. This is shown Figure 1 for an 8/6 SRM, where torque T_e, expressed as Equation (3), is dependent on current squared. It also related to the change in inductance with rotor angle $dL/d\theta$, where inductance also has current dependence, resulting in relatively non-linear Nm/A efficiencies.

$$T_e = \tfrac{1}{2}I^2 \frac{dL}{d\theta} \quad (3)$$

Established in ref. [21], the ZTR speed range of the SRM used in this research study is limited to 1080 rpm at a FLT of 25 Nm and V_{DC} of 415 V using the two phase torque sharing principle, shown in Figure 2. It is indicated by the point at

which the upper limit envelope (blue) touches the lower envelope limit (orange), which are formed by examining the boundary conditions for ZTR in SRM current profiling. This only covers 72% of the speed range at FLT along with other load torques, and limits the full power operation, with ZTR, of the SRM.

As seen in Figure 2, as speed increases, current profiles at 1080 rpm are limited by the build up of current at turn on θ_{on} and decaying to θ_{off}. If allowed a longer period of conduction ($>\tfrac{1}{2}\theta_r$), speed can be increased past this limit while maintaining ZTR at the given V_{DC}. The challenge presented is now the introduction of three-phase overlap as either the θ_{on} is advanced or θ_{off} is delayed (into low Nm/A regions). This concept is visualised in Figure 3 using a reference $\theta_{\text{on\_ref}} = 30^\circ$, $\theta_{\text{off\_ref}} = 60^\circ$ as the two-phase conduction period with Phase A as the reference. Three-phase overlap $\theta_{\text{ov}(3\phi)}$ is limited to a maximum of 15° to avoid four-phase overlap Equation (4), otherwise RMS current will be excessive for the given 8/6 SRM, either being after $\theta_{\text{off\_ref}}$ or before $\theta_{\text{on\_ref}}$. The realised $\theta_{\text{ov}(3\phi)}$ is calculated by Equation (5), where it is the sum of the shifted turn on $\theta_{\text{on}(3\phi)}$ before or after $\theta_{\text{on\_ref}}$ and shifted turn off $\theta_{\text{off}(3\phi)}$ before or after $\theta_{\text{off\_ref}}$.

$$\theta_{\text{ov}(3\phi)} \leq \tfrac{1}{2}\theta_r - \varepsilon = \tfrac{1}{2} \times 60^\circ - 15^\circ = 15^\circ \quad (4)$$

$$\theta_{\text{ov}(3\phi)} = \left(\theta_{\text{on}(3\phi)} - \theta_{\text{on}_{\text{ref}}}\right) + \left(\theta_{\text{off}(3\phi)} - \theta_{\text{off}_{\text{ref}}}\right) \quad (5)$$

Figure 4a illustrates the use of this method with $\theta_{\text{on}(3\phi)} = 30^\circ$, $\theta_{\text{off}(3\phi)} = 2^\circ$ and therefore $\theta_{\text{ov}(3\phi)} = 2^\circ$. Now the

TABLE 1 Specifications of SRM (4 kW at 1500 rpm—base speed).

Parameter	Value	Parameter	Value (mm)
No. of motor phases m	4	Rotor outer radius	45
Stator/rotor poles N_s/N_r	8/6	Thickness of rotor yoke	15
Stator pole arc/pole pitch	0.42	Motor axial length	155
Rotor pole arc/pole pitch	0.35	Stator inner radius	46
Turns per pole N	90	Stator outer radius	83
DC link voltage V_{dc}	415 V	Thickness of stator yoke	12
RMS current I_{Rated}	12.65 A	Shaft radius	15
Phase resistance R	0.8 Ω		

Abbreviation: SRM, switched reluctance machine.

FIGURE 1 Nm/A efficiency across conduction period for given 8/6 SRM.
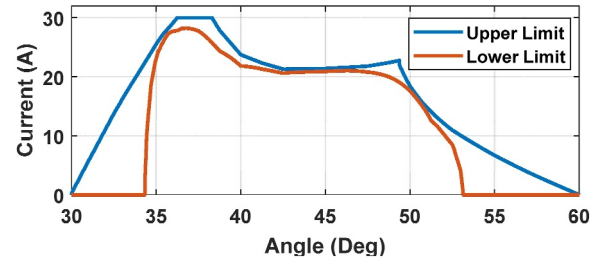

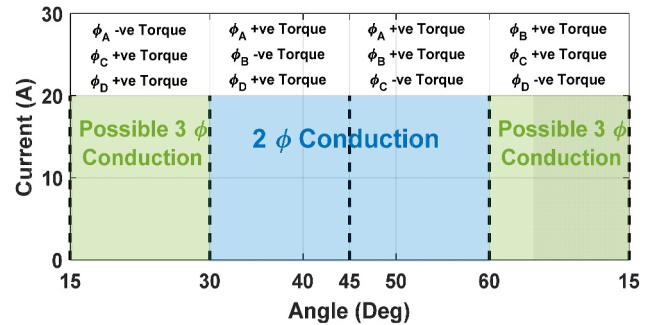**FIGURE 2** FLT two-Phase Speed Limit envelopes at 1080 rpm. FLT, full load torque.

FIGURE 3 Three-Phase conduction boundaries with reference to two-phase torque sharing.
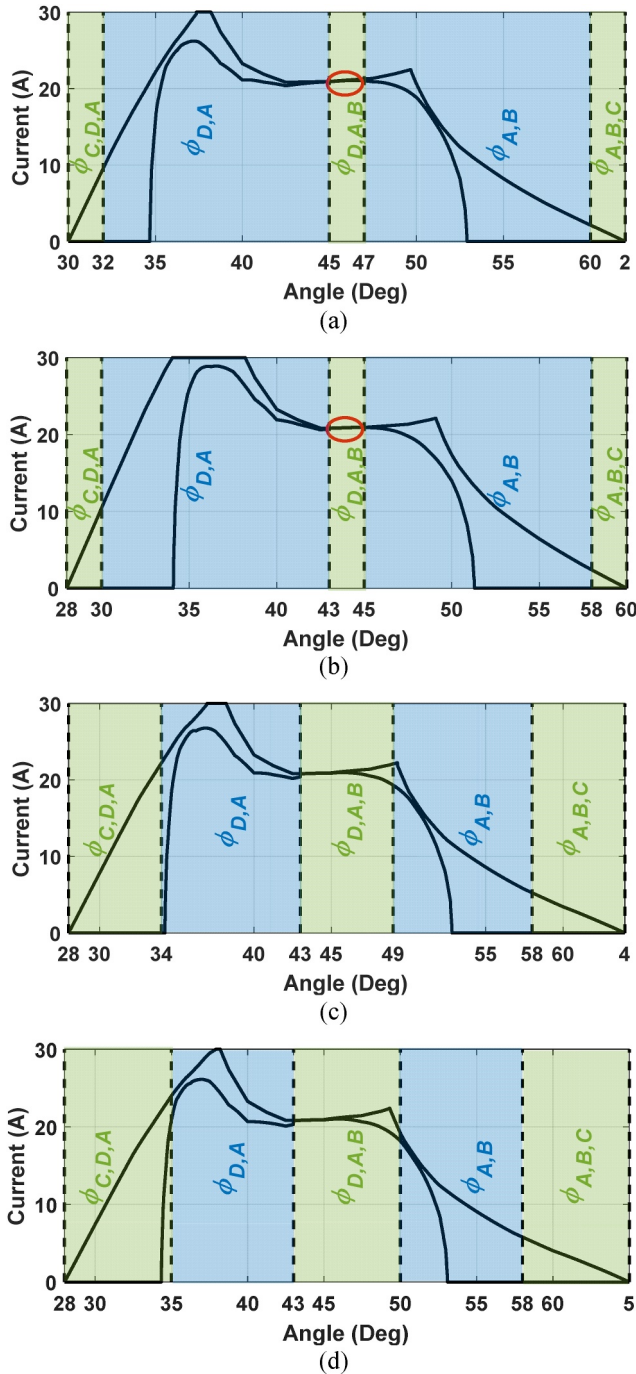
FIGURE 4 Three-Phase FLT Speed limit envelopes at: (a) 1230 rpm by delaying $\theta_{\text{off}(3\phi)}$, (b) 1130 rpm by advancing $\theta_{\text{on}(3\phi)}$, (c) 1500 rpm (base speed), and (d) 1600 rpm. FLT, full load torque.

maximum ZTR speed at FLT is extended to 1230 rpm (from 1080 rpm) by allowing a longer decay path with a delayed $\theta_{\text{off}(3\phi)}$ and an overall conduction period $\theta_{\text{cond}} = 32^\circ$. Figure 4b presents the use of this method again, this time using $\theta_{\text{on}(3\phi)} = 28^\circ$, $\theta_{\text{off}(3\phi)} = 60^\circ$ providing a $\theta_{\text{ov}(3\phi)} = 2^\circ$ but at a different angular position. Allowing a longer build up by advancing $\theta_{\text{on}(3\phi)}$ provides an increase in speed range of up to 1130 rpm. This is notably less than the equivalent $\theta_{\text{ov}(3\phi)}$ in Figure 4 due to the requirements of excessive peak currents to

produce the majority of FLT in the 35°–38° region above the SRMs current limit. Note that due to this extension of a prospective profile into the negative torque production region, compensation of the additional negative torque must be considered. This is done by allowing the control phase to produce torque greater than FLT, as highlighted in red where the upper envelope boundary is increased by the maximum amount of compensation it may need to provide during three-phase overlap in both Figures 4a,b.

Utilising this method, Figure 4c shows an example of a three-phase profiling envelope for the SRM peak power point at 1500 rpm with FLT. This example makes use of both an advanced $\theta_{\text{on}(3\phi)} = 28^\circ$ and delayed $\theta_{\text{off}(3\phi)} = 4^\circ$, collectively resulting in an $\theta_{\text{ov}(3\phi)} = 6^\circ$. This is only an example of a combination of $\theta_{\text{on/off}(3\phi)}$ that can yield feasible current profiles at the given speed; multiple combinations of limit envelopes exist at each speed for a given SRM. An added benefit of the method is that it can be proven that ZTR operation at FLT can be achieved above the rated speed and power of the machine as illustrated in Figure 4d at 1600 rpm with $\theta_{\text{ov}(3\phi)} = 7^\circ$. The limitation on achieving this operating point for a prolonged period though may not be associated with the machine electrical parameters but external factors such as thermal or mechanical limitations.

With the concept of intentionally utilising more than two-phase overlap in an SRM to harness the full speed range and power of the machine with ZTR, a current profiling-based approach can be used to obtain current profiles which satisfy the ZTR and V_{DC} limits while optimising RMS current.

3 | PROPOSED THREE PHASE GENETIC ALGORITHM DESIGN FOR SWITCHED RELUCTANCE MACHINE CURRENT PROFILING

The GA approach to current profiling in ref. [21] is limited to two-phase torque sharing with the given 8/6 SRM and is applicable to any multi-phase SRM. This section proposes an adaptation of the algorithm, where all stages of the algorithm are modified for the consideration of three-phase overlap. Below the two-phase speed limit, three-phase overlap is inefficient (RMS current wise). When considering optimally minimal RMS currents, any θ_{cond} that is greater than 30° (three-phases) includes the production of negative torque in one additional phase along with the two other phases conducting. This is opposed to two-phase torque sharing where at most one phase will produce negative torque while the other is producing positive torque.

The GA functions in principle by aiming to optimise three variables, being ZTR, minimal RMS current, and DC voltage to the available V_{DC}. In designing the GA, two of these variables can be solved as prerequisites for any created current profile and maintained through the algorithm process. TR as a variable can be eliminated by ensuring every 'gene' of a population current profile, which are the overlapping currents at each angular point, collectively produce FLT (with

ZTR). DC voltage usage can be solved by ensuring that population members at generation already are within DC voltage limits, and any stage of the GA must also consider the available $di/d\theta$ between any two genes in a population member if one is altered. With this, the GA can solely optimise the RMS current. The GA functions as follows: population generation is carried out once and then crossover, mutation, evaluation, and selection stages are performed for 5000 'generations'. An illustration of the algorithms flow is in Figure 5. At the selection stage of each generation, 250 candidate current profiles are chosen from a pool of 750 created by crossover and mutation, where candidates with an RMS current closer to the theoretically optimal RMS $I_{rmsOptimal}$ are favoured. The number of generations are chosen as a reasonable estimation for the amount for iterations that the algorithm takes to converge on an optimal
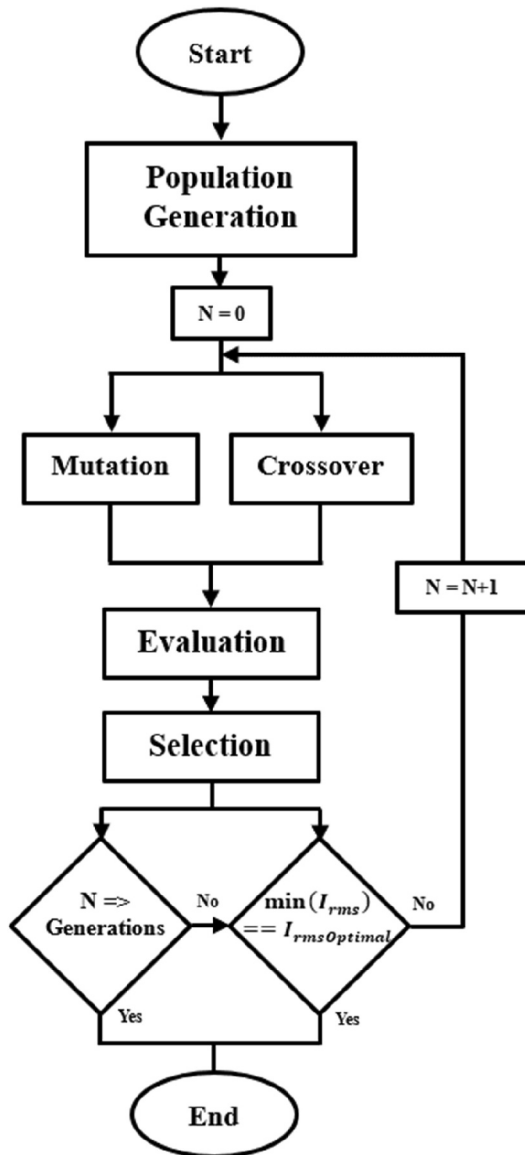
solution while in the design phase. The number of crossovers and mutations provide a good pool of current profile variations, given that the actual available range of practical solutions is not large when considering Figure 2 or Figure 4, when compared to other possible applications of a GA.

3.1 | Population generation

GA population generation consists of procedural, random generation of current profiles within the boundaries imposed by the limit envelopes, with an example given at 1200 rpm in Figure 6. It is performed at an angular increment θ_{step} of 0.1°, for a balance between ZTR profile accuracy and maintaining reasonable computational demand for the algorithm itself. When iterating, phase pairings are chosen from a grid of currents at 500 solutions per increment, linearly spaced from the upper to lower envelope bounds for each of the three phases Equation (6). Each of these phase 'pairings' or 'trios' in the three-phase overlap region produce ZTR collectively at each increment, where the currents are converted to torques using a $T - I - \theta$ LUT, as shown in Figure 7a, expressed as $T(I, \theta)$. Each given phase ϕ_k is separated by the maximum θ_{ov} $_{(3\phi)}$ and in narrower regions of the envelope it is seen that currents selected for the profiles become alike with the limited number of variations available in solutions. Once
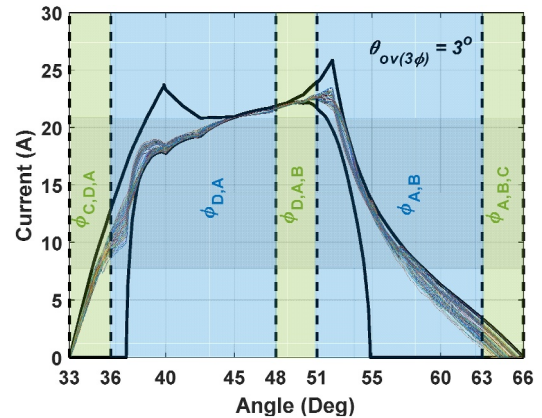

FIGURE 6 GA population generation at 1200 rpm. GA, genetic algorithm.

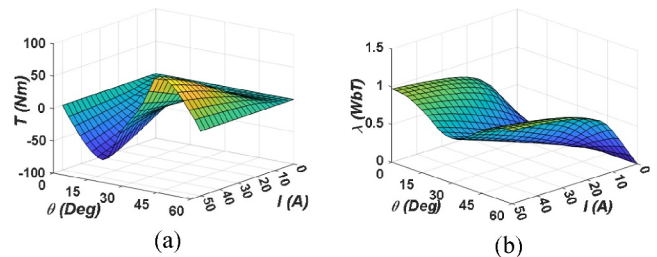**FIGURE 5** Overview of the proposed GA process. GA, genetic algorithm.

FIGURE 7 Ansys Maxwell FEA 4 kW 8/6 SRM data relating: (a) $T - I - \theta$ and (b) $\lambda - I - \theta$. FEA, finite element analysis; SRM, switched reluctance machine.

currents are chosen at a given point, they are converted to values of flux linkage λ using a $\lambda - I - \theta$ LUT for the SRM, as shown in Figure 7b, expressed as $\lambda(I, \theta)$. The maximum value of the rate of change of flux linkage $\frac{d\lambda}{d\theta}$ is then calculated using Equation (7), where ω is the SRMs electrical speed and R_{Cu} represents the SRMs phase resistance. This value is then added and subtracted to phase flux linkage values λ_{ϕ_n} (Equation 8), where new values establish a range where the profiles next phase values can randomly be chosen at the next angular increment (Equation 9) from the previous angle θ_n. The feasible range is reverted to currents and matched to indexed pairings in the current solutions grid if valid combinations exist within the range. This provides a selection of pre-calculated ZTR phase values, maintaining V_{DC}. In the case of any partially constructed profile having no possible current combinations that can be added in the next angular increment, the profile is deleted, and the process is restarted. Revisiting Figure 8, the population is generated with 250 initial candidates where profiles have a similar general shape. As speed increases, this is likely given the lack of $d\lambda/d\theta$ and the FLT requirements meaning that there are realistically limited variations available that allow the profile to build up and decay while continuing to provide ZTR. Stated in the prior section, this is also not the only $\theta_{ov(3\phi)}$ and combination of $\theta_{on/off(3\phi)}$ available. Multiple GA iterations may be required, depending on the speed, as different $\theta_{ov(3\phi)}$ and $\theta_{on/off(3\phi)}$ can yield similar RMS currents near $I_{RMSOptimal}$.
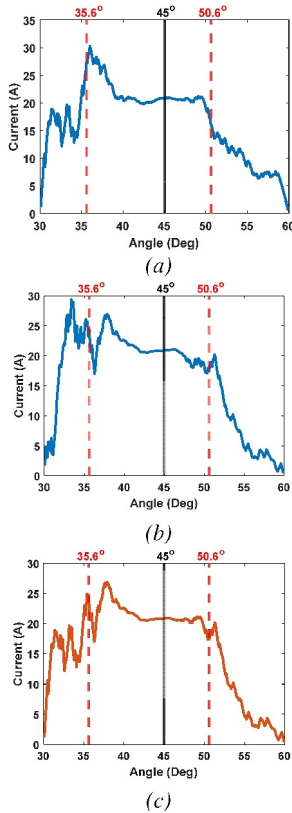
$$\phi_{1,2} = \begin{bmatrix} \lambda, I_{Upper(33°,48°)} & \cdots & \lambda, I_{Upper(48°,63°)} \\ \vdots & \ddots & \vdots \\ \lambda, I_{Lower(33°,48°)} & \cdots & \lambda, I_{Lower(48°,63°)} \end{bmatrix}$$

$$\phi_3 = \begin{bmatrix} \lambda, I_{Upper(63°)} & \cdots & \lambda, I_{Upper(66°)} \\ \vdots & \ddots & \vdots \\ \lambda, I_{Lower(63°)} & \cdots & \lambda, I_{Lower(66°)} \end{bmatrix} \tag{6}$$

$$\frac{d\lambda}{d\theta} = \frac{V_{DC} - IR_{Cu}}{\omega} \tag{7}$$

$$\lambda_{\phi_n} = \lambda\left(I_{\phi_k\theta_n}, \theta_n\right) \tag{8}$$

$$\lambda_{\max\left(\phi_k,\theta_n+\theta_{step}\right)} = \lambda_{\phi_k\theta_n} + \frac{d\lambda_{\max}}{d\theta} \\ \lambda_{\min\left(\phi_k,\theta_n+\theta_{step}\right)} = \lambda_{\phi_k\theta_n} - \frac{d\lambda_{\max}}{d\theta} \tag{9}$$

3.2 | Profile crossover

The GA Crossover stage consists of 'splitting' two separate population members at specific points or point into two or more segments. These segments are then recombined into different, new population members and the original population members are discarded. The GA design proposed in this paper functions in a similar manner where an angular point and its respective two-phase angle and/or three-phase angle are randomly selected for two 'parent' current profiles. The parents are then split at the crossover and 'offspring' profiles are created if criteria are met. The first considerations that are made at crossover are towards the preservation of ZTR when splitting and recombining current profiles. FLT is provided at each stored current pair, and this is not altered in the crossover process. In the case of a three-phase profile, the three-phase overlap region total torque is verified after crossover, and any changes are compensated for in the highest Nm/A phase. The main criteria that must be met is the $d\lambda/d\theta$ at the crossover points in the profiles. This is because at the crossover angles, Equation (9) is used to determine the maximum and minimum flux linkage and therefore current achievable by the profile at the next angular increment. The next angular increment will be a section of the opposite parent profile, and if this change in current at any of the crossover points is not achievable with the given V_{DC}, the crossover will not occur. Instead, a different random angle will then be selected, and the process will be repeated until criteria is met and profile crossover can occur.

An example of this process is given in Figure 8 at low speed, two-phase overlap conditions. A crossover point selected at $35.6°$ and $50.6°$ ($35.6° + \theta_{ov}$), and given the low speed, a comparatively low $d\lambda/d\theta$ is required and the crossover points are valid between the profiles. The child profile

FIGURE 8 Crossover stage performed at 200 rpm for two population members: (a) Parent 1, (b) Parent 2, and (c) offspring.

(Figure 8c) is composed of sections of the first parent profile (Figure 8a) before the crossover point and the second parent profile (Figure 8b) after the crossing point.

As speed increases, profiles require an increasingly defined shape from generation, as shown in Figure 9. Crossover at these speeds therefore produces less variation in profile structure given the requirements of a strict current build up and decay. Figure 9 illustrates an example of crossover at a higher speed of 1200 rpm. The crossover is selected at 41° and 56° and both parent profiles (Figure 9a,b) have relatively similar forms. The child profile (Figure 9c) therefore still resembles both profiles, with the crossover making a new profile but with only minor adjustments in the new shape as opposed to Figure 8 for the exact same crossover process.

3.3 | Profile mutation

For the mutation stage, a single gene in a population member is randomly selected. From this the value of the selection is 'mutated' by changing its value randomly and reinserting it back into its original place within the population member, but variations exist. Applying this to SRM current profiles, such as crossover a random angle θ_{Mu} is selected within the current profile with its respective phase pairing. Both ZTR and V_{DC} need to be verified during this stage given the values of

currents are specifically altered as opposed to the crossover stage where no new currents are generated. Focussing on one phase first, the chosen θ_{Mu} next and prior current values are recorded. Equation (9) is used with each of these values to establish the range of valid currents at the mutation angle which satisfy the available V_{DC}. If the ranges established overlap for each phase's mutation angle given in Equation (10), a mutation is possible within V_{DC} limits.

$$\lambda_{\max\,(\theta_{\mathrm{Mu}}-\theta_{\mathrm{step}})} \geq \lambda_{\max(\theta_{\mathrm{Mu}}-\theta_{\mathrm{step}})}, \lambda_{\max(\theta_{\mathrm{Mu}}-\theta_{\mathrm{step}})} \leq \lambda_{\max(\theta_{\mathrm{Mu}}-\theta_{\mathrm{step}})}$$
$$\text{or}$$
$$\lambda_{\min(\theta_{\mathrm{Mu}}-\theta_{\mathrm{step}})} \geq \lambda_{\min(\theta_{\mathrm{Mu}}-\theta_{\mathrm{step}})}, \lambda_{\min(\theta_{\mathrm{Mu}}-\theta_{\mathrm{step}})} \leq \lambda_{\max(\theta_{\mathrm{Mu}}-\theta_{\mathrm{step}})}$$
$$\text{or}$$
$$\lambda_{\max\,(\theta_{\mathrm{Mu}}+\theta_{\mathrm{step}})} \geq \lambda_{\max(\theta_{\mathrm{Mu}}-\theta_{\mathrm{step}})}, \lambda_{\max(\theta_{\mathrm{Mu}}-\theta_{\mathrm{step}})} \leq \lambda_{\max(\theta_{\mathrm{Mu}}-\theta_{\mathrm{step}})}$$
$$\text{or}$$
$$\lambda_{\min(\theta_{\mathrm{Mu}}+\theta_{\mathrm{step}})} \geq \lambda_{\min(\theta_{\mathrm{Mu}}-\theta_{\mathrm{step}})}, \lambda_{\min(\theta_{\mathrm{Mu}}-\theta_{\mathrm{step}})} \leq \lambda_{\max(\theta_{\mathrm{Mu}}-\theta_{\mathrm{step}})}$$
$$\tag{10}$$

$$I_{\phi_{k+1}(\mathrm{Max/Min})} = I\left(T_{\phi_{k+1}(\mathrm{Max/Min})}, \theta_{\mathrm{Mu}} + 15°\right) \tag{11}$$

$$T_{\phi_{k+1}(\mathrm{Max/Min})} = T_{\theta_{\mathrm{Mu}}} - T\left(I_{\mathrm{Mu}(\mathrm{Max/Min})}, \theta_{\mathrm{Mu}}\right) \tag{12}$$

Considering the torque production of the mutation, the initial θ_m produces a set value of torque which satisfies FLT when either the two, or three conducting phases are combined. This means that when mutation is being considered the value of torque produced collectively at θ_m must be reproduced given a third phase conducting would require the initial two phases to produce greater than FLT to compensate for the negative torque production. This provides a second set of current ranges $I_{\phi_{k+1}(\mathrm{Max/Min})}$ given by Equation (11) once V_{DC} is verified, where the maximum and minimum flux range currents $I_{\mathrm{Mu}(\mathrm{Max/Min})}$ are converted into their respective torques $T_{\mathrm{Mu}(\mathrm{Max/Min})}$. This establishes a torque range $T_{\phi_{k+1}(\mathrm{Max/Min})}$ defined by Equation (12) in the torque sharing phase ($\theta_{\mathrm{Mu}} + 15°$) which will satisfy the initial torque production $T_{\theta_{\mathrm{Mu}}}$, which is converted back to current using the LUT in Figure 9a in reverse. Once both the flux linkage and torque ranges are established, and an overlap exists between them in each phase (ϕ_k, ϕ_{k+1}) a mutation can be carried out which satisfies GA conditions. If at any point either a flux range cannot be established or the two ranges have no overlap, a mutation is not possible at the given point and a new one is selected.

A visualisation of the process is shown in Figure 10 at 1200 rpm. Firstly, a mutation point is selected at 36.6° and 51.6° which in this case two phase conduction occurs. In each phase, the range of available change in flux linkage is established with an overlap between $\lambda_{\max(\theta_{\mathrm{Mu}}-\theta_{\mathrm{step}})}$, $\lambda_{\min(\theta_{\mathrm{Mu}}+\theta_{\mathrm{step}})}$ in the first incoming phase and again, $\lambda_{\max(\theta_{\mathrm{Mu}}-\theta_{\mathrm{step}})}$, $\lambda_{\min(\theta_{\mathrm{Mu}}+\theta_{\mathrm{step}})}$ in the outgoing phase. From this, the ZTR range is established
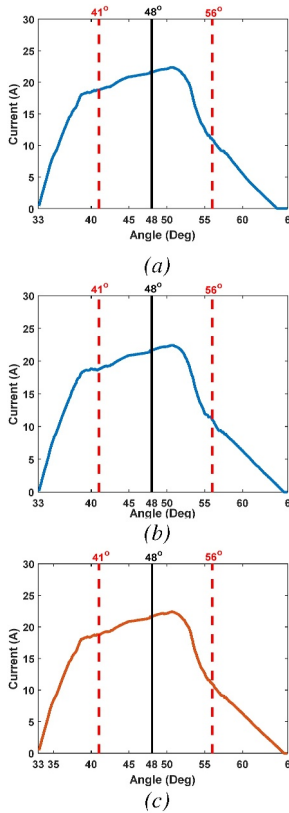

FIGURE 9 Crossover stage performed at 1200 rpm for two population members: (a) Parent 1, (b) Parent 2, and (c) offspring.
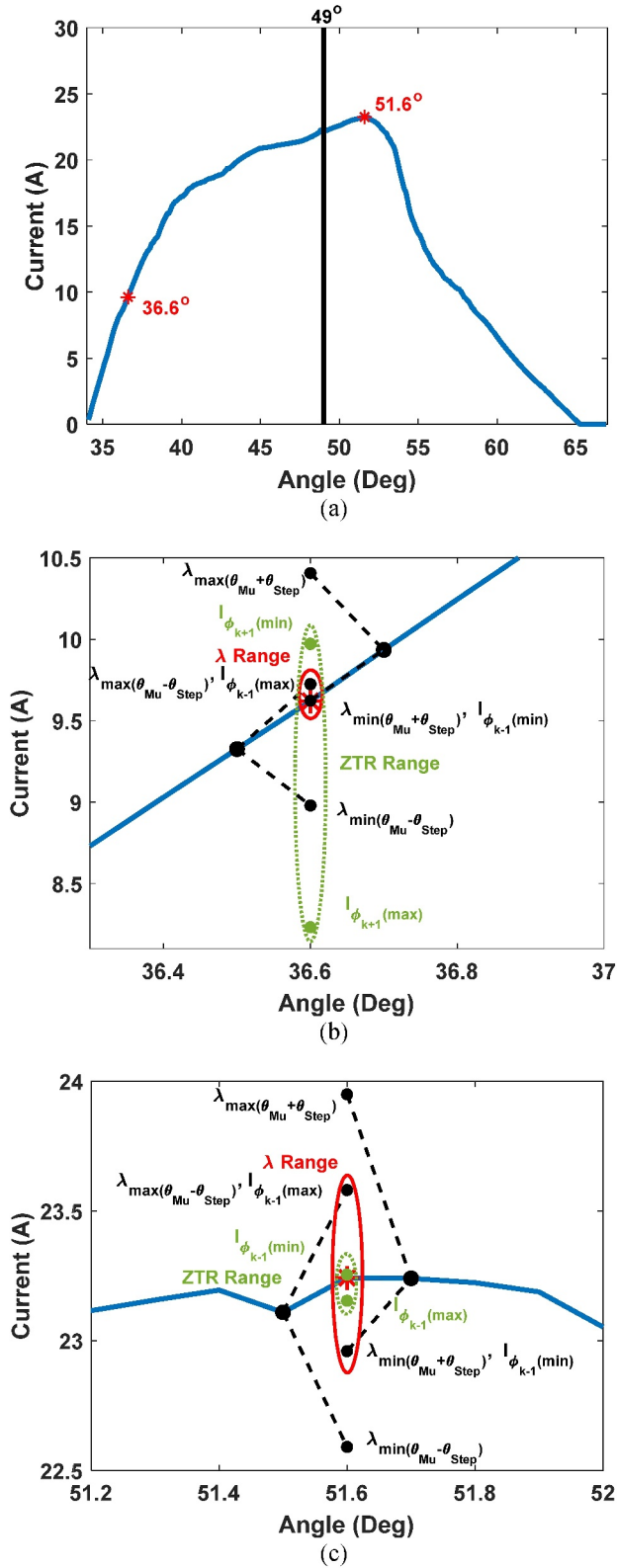
FIGURE 10 Mutation stage carried out at 1200 rpm: (a) The population member, (b) incoming phase mutation, and (c) outgoing phase mutation.

using Equations (11) and (12) in either phase using the other phases flux linkage range. In the incoming phase, the valid mutation is bounded by torque production requirements,

whereas in the outgoing phase the valid mutation is instead bounded by the available V_{DC}. At higher speeds, it is expected that during mutation, one phase will dominate the available mutation range. This is because with the overlap between phases, one phase out of the two predominate phases (even for three phase overlap) will either be decaying or building up. This limits the available range for mutation in that phase due to the V_{DC} restriction. In the example shown in Figure 10, the incoming phase is building up current and creates only a small range for mutation. This is while the outgoing phase is in a high Nm/A efficiency region, and therefore has a wider range current it could be mutated to in its flux linkage range but instead is limited to the incoming phase ZTR range in order to maintain ZTR.

3.4 | Profile evaluation and selection

How a GA evaluates its progress is determined by its design, based upon its objective and how it calculates each population members 'fitness' as it relates to these objectives. This can be complex if presented with multi-objective problems given that issues can arise such as biasing towards certain objectives over others which results in non-optimal solutions. As previously discussed, the SRM current profiling problem in principle is a multi-objective problem concerning the preservation of ZTR, V_{DC} usage limit and RMS current minimisation. Through the design of this proposed GA, the problem is simplified to only being concerned with RMS current minimisation of each profile with any candidate profile always maintaining ZTR and V_{DC} limits while the GA operates. This results in a simple objective function, as expressed by Equation (13), based upon the absolute proximity of each profile's RMS current I_{rms} to the theoretically lowest RMS current $I_{rmsOptimal}$ possible for a FLT demand, V_{DC} and parameters of the 4 kW 8/6 SRM calculated using the method proposed in ref. [21].

$$\text{Fitness} = \left(1 - \frac{|I_{rmsOptimal} - I_{rms}|}{I_{rmsOptimal}}\right) \quad (13)$$

Profiles which pass from each generation while the GA iterates are selected using 'roulette wheel' selection. This selection operates by summing every population member's fitness as a collective 'wheel' value with every individual member's fitness representing a segment of said wheel. The probability of selection is taken by dividing the individual fitness values by this value. This means members with larger fitness values have a larger segment and chance of selection based upon the cumulative probability of selection from the population. With these probabilities calculated, the selection process is run for however many members are desired in the new population. Each time a population member is selected, the probabilities are recalculated, and when all selections are made, the remainder are discarded with the GA iterating to the next generation.

4 | SIMULATION RESULTS

The GA method described in the previous section is implemented using MATLAB script and is run using an initial population of 250 current profiles for 5000 generations, producing profiles in 100 rpm increments from 1100 to 1500 rpm, with an average calculation time of 0.83 s per generation and utilising an average of 4.9% of a 4.7 GHz CPU. Results for the remainder of the speed range (0–1000 rpm) already exist, as presented in ref. [21], where only two-phase overlap is required, but are utilised as part of the control scheme introduced in this section. An example of the GA progression is given in Figure 11. Figure 11a shows the overall progression in terms of fitness, while Figure 11b illustrates the initial results set of the algorithm, which shows the profile that is initially generated with the lowest RMS current and therefore the highest fitness. The algorithm then develops fitness rapidly with a steep ascent for an initial 300 generations. Once it reaches this point, the slope begins to saturate, indicating that after a certain number of clear modifications to the profiles, reaching RMS currents closer to the theoretical optimal requires more generations. In this region where the increase in fitness is slowing, it can also be seen that while across the whole period fitness is still increasing, the GA alternates between losses in fitness where certain local minima may be discarded or certain pathways for optimisation are discarded by chance. The final result set in this example is present in Figure 11c, where a reduction of RMS current of 0.9% (0.1 A) relative to $I_{\text{rmsOptimal}}$ of 11.129 A.

4.1 | Optimal profiles

Figure 12 illustrates the products of executing the GA in 100 rpm increments from 1100 to 1500 rpm, with the three phase overlap characteristics being highlighted in Table 2. In this speed range, three phase overlap is necessary to allow the build up and decay of enough current for FLT production and $\theta_{\text{ov}(3\phi)}$ increases with speed. This overlap is seen more in the decay path of the profiles, where to maintain the majority of FLT production in the most efficient Nm/A regions shown in Figure 1 (40°–50°), decay typically begins after 53°. θ_{on} also begins to advance for the same reasons, where build up is limited by the required $d\lambda/d\theta$ and requires a longer conduction period in lower Nm/A regions to reach the same current levels. As speed increases, the decay path becomes notably longer (further delayed θ_{off}) for the same advanced θ_{on}, introducing more efficient regions of negative torque production for greater periods of the conduction period. This contributes to an RMS current increase but is an acceptable trade to avoid excessive peak currents on the initial profile build up. More importantly, across the full SRM speed range from 0 to 1500 rpm, RMS current is maintained below the I_{rated} given in Table 1. Examining torque production during three-phase overlap, it can be seen that the total average torque collectively between the phases is maintained within 1% of
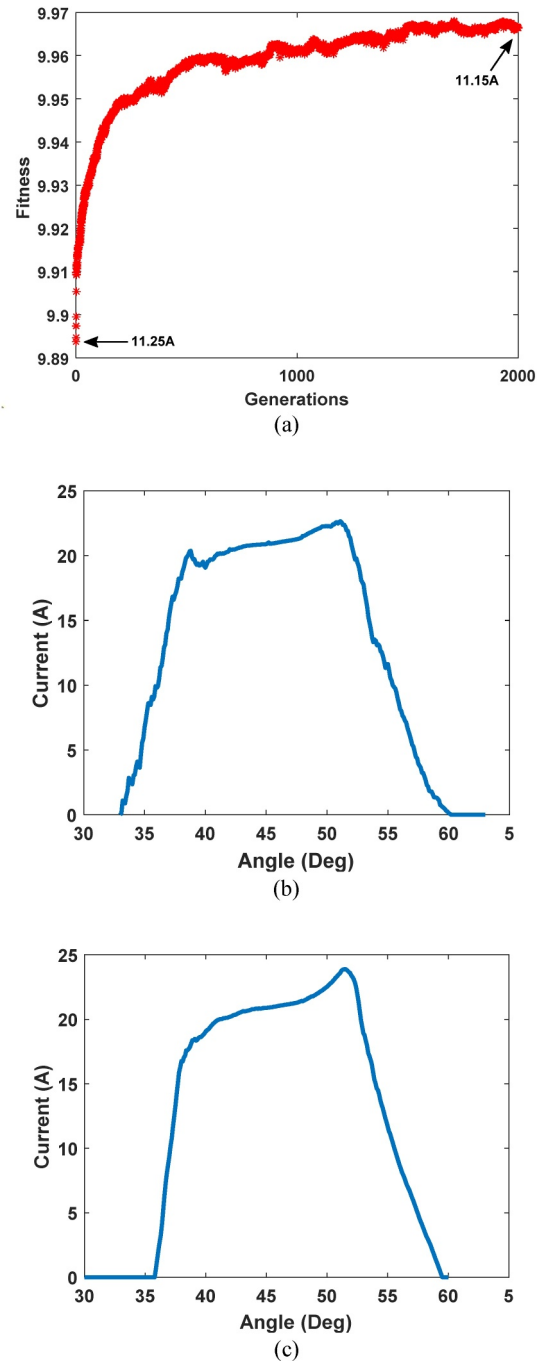

FIGURE 11 Progression of GA. (a) Fitness across generations with (b) initial result set and (c) final result set. GA, genetic algorithm.

FLT demand as the two positive torque producing phases (A and B) combine to produce greater than FLT for compensation of phase D to maintain the elimination of commutation TR as can be seen with the peak and average values of TR being mathematically maintained below 1%. As speed increases, average torque production shifts towards phase B from phase A. For reference, phase B in this case is the portion of the profile near the unaligned position, where increasing speed causes a longer build up of current, and therefore more torque on average.

Noted that for optimal efficiency, currents at the aligned position (60°) will increase with speed as a greater tail off current is created. These are given in Table 3 and begin at 700 rpm, which up to 1100 rpm are not given in Figure 12 but are present in Ref. [21]. At alignment (60°) tangential Nm/A is zero but radial force Nm/A is a maximum. The tail current produced radial force causes stator deformation resulting in acoustic noise and vibration in the machine. The aligned current approaching base speed is not significant, and below 700 rpm, zero current (radial force) exists at alignment.

4.2 | Switched reluctance machine control scheme

Using the proposed GA, a control scheme can be created for SRM speed and linear torque control. The 8/6 SRM described in Table 1 is modelled per phase as shown in Figure 13. Phase torque T_{Ph} is produced calculated from the $T - I - \theta$ LUT in Figure 7a, where I is acquired from a $\lambda - I - \theta$ LUT in Figure 6b, inferring λ from the integral of the phase rail voltage. From each phase, the total instantaneous electrical torque T_e is given as a sum of all phase torques, T_{Ph} as given by Equation (14).

$$T_e = \sum_{1}^{n} T_{\text{ph}}(I, \theta) \qquad (14)$$

The SRM mechanical model is expressed by Equation (15), where ω_m is the mechanical speed, T_L is the load torque, J is the rotor inertia constant, and B_{fric} is the friction coefficient.
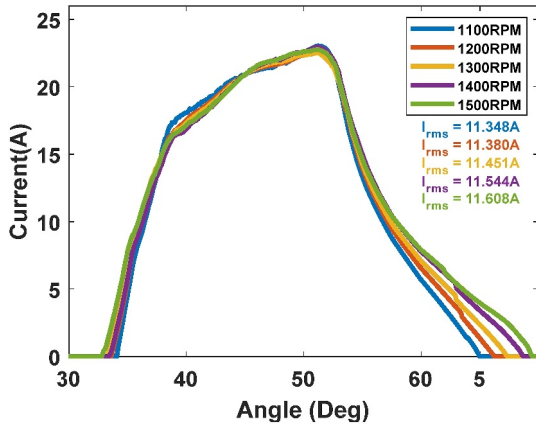
$$J \frac{d\omega}{dt} = T_e - T_L - B_{\text{fric}}\omega \qquad (15)$$

To operate the SRM, the control scheme implementation of the GA profiles is similar to TSF control schemes. Along with the profiles generated for FLT, further profiles are generated across the SRMs rated speed range, for example, 0.75, 0.5 and 0.25 of FLT. These current profiles shown in Figure 14a for FLT and can also be represented as torques, where Figure 14b illustrates the torque profiles for FLT from 0 to 1500 rpm.

This range of current profiles across the various FLT values are stored in a 3D $I_{\text{ref}} - \omega_{\text{ref}} - T_{\text{ref}} - \theta$ LUT placed

TABLE 3 Aligned currents with each speed at FLT.

Speed (rpm)	Aligned current (A)
700	1.64
800	2.83
900	4.03
1000	4.85
1100	5.69
1200	6.52
1300	7.08
1400	7.77
1500	7.89

Abbreviation: FLT, full load torque.

FIGURE 12 GA profiling results from 1100 to 1500 rpm. GA, genetic algorithm.
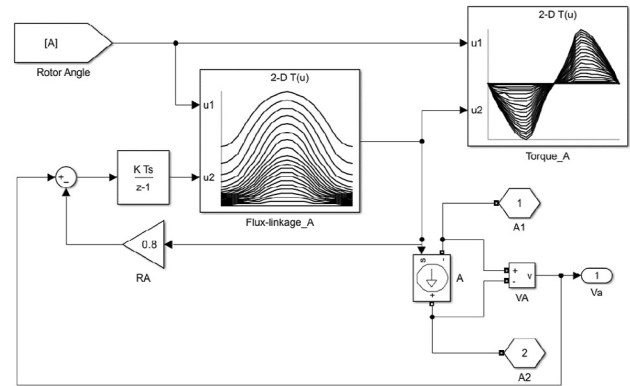
FIGURE 13 Simulink model of an SRM phase. SRM, switched reluctance machine.

TABLE 2 Three phase overlap characteristics from 1100 to 1500 rpm.

Speed (rpm)	$T_{(\text{avg})\phi_A}$ (Nm)	$T_{(\text{avg})\phi_B}$ (Nm)	$T_{(\text{avg})\phi_D}$ (Nm)	$T_{(\text{avg})}$ Total (Nm)	%TR$_{\text{pk}}$ (Commutation TR)%	%TR$_{\text{avg}}$ (Commutation TR)%	θ_{ov} (3ϕ)(°)	θ_{cond} (°)
1100	25.01	0.01	−0.02	25.02	0.08	0.02	0.9	30.9
1200	24.53	0.57	−0.10	24.99	0.16	0.02	2.7	32.7
1300	23.85	1.37	−0.22	25.01	0.53	0.08	4.1	34.1
1400	22.83	2.55	−0.36	25.02	0.43	0.06	5.2	35.2
1500	21.87	3.68	−0.54	25.02	0.41	0.04	6.7	36.7

within the control loop shown in Figure 15 that outputs a reference current value I_{ref} based upon the speed target ω_{ref}, required torque to settle speed error T_{err} and rotor position θ. This control consists of a speed control PI loop with an inner current control loop where the LUT is situated. The phase current error I_{err} is then fed to hysteresis band current control which produces pulse width modulation to be fed onto the drive converter. By implementing this, the SRMs non-linear torque production can be controlled linearly, where any torque increment in Figure 15 can be linearly translated into current increments without excessive calculation burden. For the 8/6 configuration, it is necessary that for 3-phase overlap of currents, each phase requires its own independent converter switches. This means that converter configurations such as those presented in refs. [22, 23], where switches are shared between orthogonal phases to reduce the number of components, a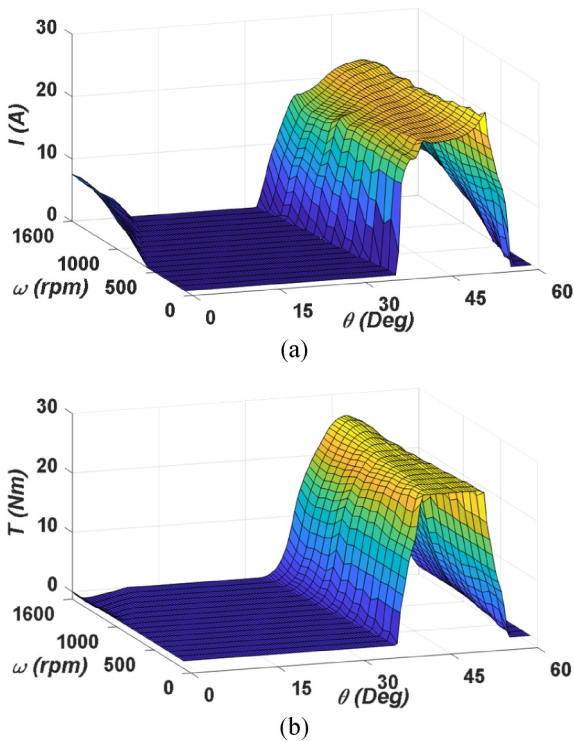re not compatible. Instead, the conventional asymmetric half bridge converter is used to allow the three-phase overlap and soft switching while operating the SRM.
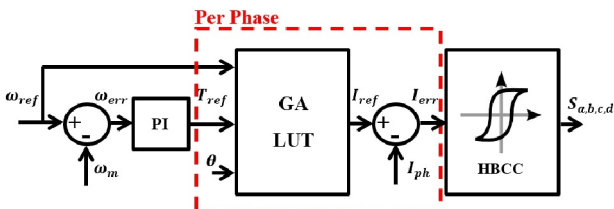
Figure 16 shows the results of the modelled SRM simulated with this control scheme, using a switching frequency of 20 kHz and a sampling time of 10 μs. The SRM is loaded with FLT and accelerated from start-up to 1100 rpm, operated at this steady state and further accelerated to a new steady state at maximum power at 1500 rpm as illustrated in Figure 16a for speed and Figure 16b for torque over a period of one second. This demonstrates the proposed scheme's speed control performance, controlling the SRM across its speed range using the GA current profiles, also without notable TR during dynamic portions of the SRMs response (and near ZTR during steady state periods).

Shown in Figure 16c,d are the steady state current and torque waveforms respectively for the SRM operating at 1500 rpm and FLT from 0.6 to 1 s in Figure 16a. Phase A is taken as a reference in this case for the rotor position where the profile has a realised θ_{cond} of 36° in Figure 16c, displaying a significant $\theta_{ov(3\phi)}$. Commutation TR is eliminated at this speed and overlap, where Figure 16d shows a resultant commutation TR of less than 1% of the FLT value, while switching frequency-based ripple accounts for a TR of 6%. This produces a peak negative torque value of −1.45 Nm approaching θ_{off}, requiring a peak two-phase positive torque production of 26.45 Nm. The waveform RMS current values are maintained at the value illustrated in Figure 11, accomplishing the objectives of ZTR and minimal RMS currents below the SRMs rating; this shown that by accomplishing these two objectives, the profiles are produced within the V_{DC} limits that have been outlined.

Revisiting a dynamic portion of the SRMs response, Figure 16e,f present the currents and torques respectively during the initial acceleration from 0 to 1100 rpm highlighted in Figure 16a. No phase is taken as a reference here and the waveforms are displayed against time. This portion of operation demonstrates the GA control schemes ability to interpolate between torques and speed without adverse commutation TR or increase to RMS current as the machine is accelerated and torque loaded gradually. The GA LUT utilises basic linear interpolation methods. This shows a good correlation between the current profiles at the various speeds/torques as a generalised form, which again lends itself to its ability to provide linear torque control. This general shape of current profile demonstrates the capability to maintain minimal RMS currents and TR throughout the SRMs speed range between bespoke current profiles.

FIGURE 14 GA profiles from 0 to 1500 rpm: (a) Currents and (b) torques. GA, genetic algorithm.

FIGURE 15 GA LUT control loop. GA, genetic algorithm; LUT, lookup table.

5 | DISCUSSION

The GA design and its resultant control scheme has been presented along with its merits. Many examples of control schemes in literature exist which can be compared. This

includes control methods which can be considered as classical in SRM control and much newer strategies, which build on classical methods.
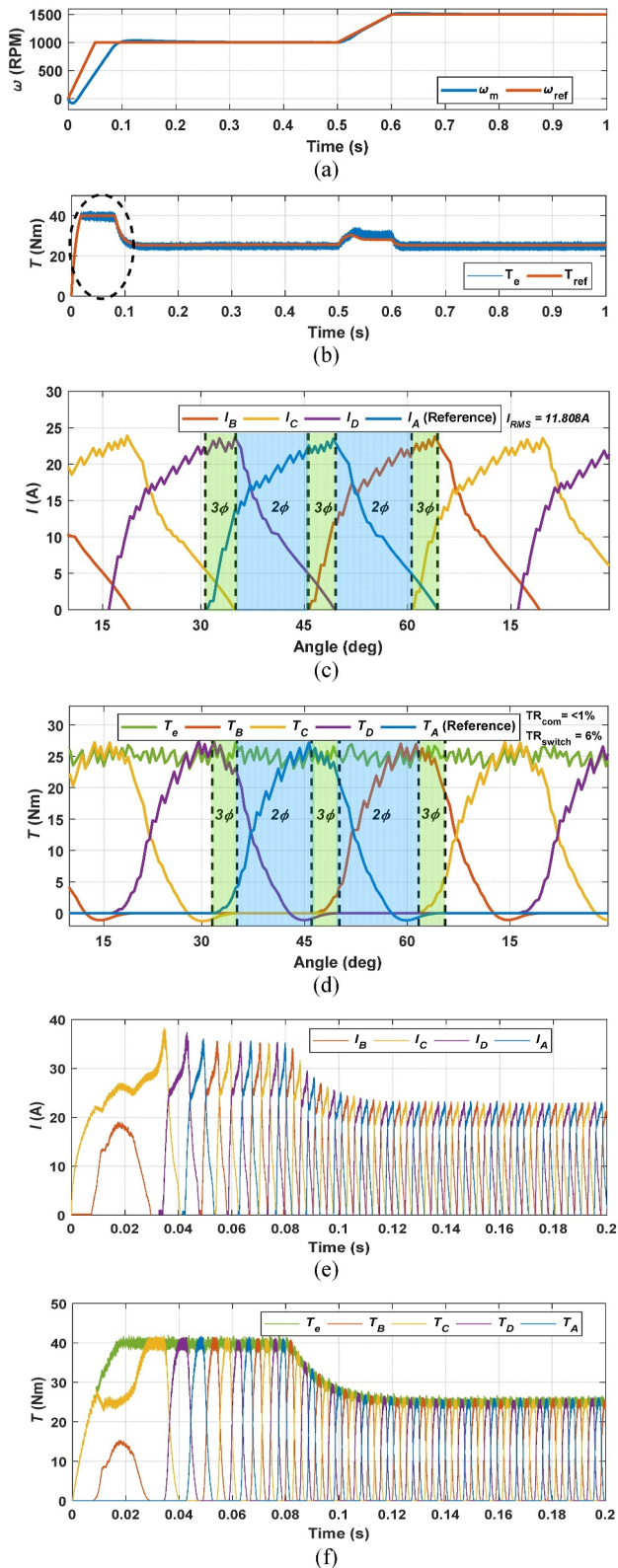

FIGURE 16 Results of SRM Drive: (a) Speed and (b) torque, 1500 rpm steady state, (c) currents and (d) torques, 0–1100 rpm, and acceleration (e) currents and (f) torques. SRM, switched reluctance machine.

5.1 | Comparison with cosine TSF

Figure 17 presents the results at 1500 rpm using a standard Cos TSF at FLT. Note that the proposed GA design produces a RMS current of 11.608 A compared to 12.310 A for the Cos TSF, at 1500 rpm. At this speed, the Cos TSF is pressed beyond the limits of two-phase overlap and inherently cannot compensate for the limited amount of available V_{DC} to build up and decay from FLT production. This results in a commutation TR of 7% in the waveform as would be expected as torque sharing between phases begins, along with and an increase in RMS current and switching ripple of 6%. This is because the Cos TSF cannot calculate an efficient torque sharing phase commutation for $\theta_{cond} > 30°$ without some form of modification, given TSFs in principle cannot operate beyond the two-phase overlap. Conversely, the GA accounts for the requirement of the three-phase overlap, and effectively maintains ZTR and minimal RMS current while operating at higher speeds. It continues to utilise delayed θ_{on} and θ_{off} to allow the majority of FLT production in the most efficient Nm/A regions in exchange for conduction in the second phase beyond $60°$. This introduces an acceptable amount of negative torque given the resultant RMS current and its proximity to theoretical optimal of 11.129 A.

5.2 | Comparison as a control scheme

Typically, control schemes will implement some form of reduction in TR, since this is a challenge that must be overcome for many applications to use an SRM. Accompanying this, they may also seek to reduce RMS current, peak
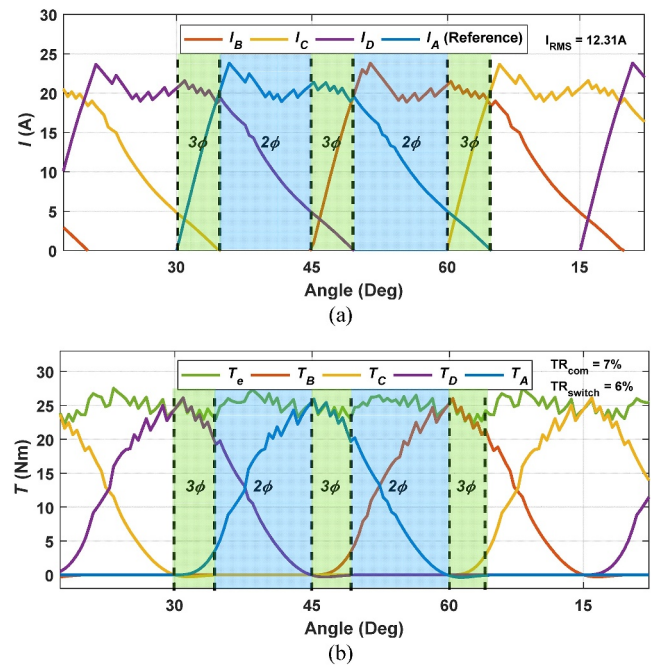

FIGURE 17 Results of Cos TSF at 1500 rpm. (a) Currents and (b) torques. TSF, torque sharing function.

current, or extend speed range. Table 2 presents a comparison between various recent SRM control scheme publications. While publication [15, 24–27] results are simulated for a specific SRM configuration (including the GA scheme) it does not mean that they are limited to that configuration as such. For example, the GA method can be applied to any SRM with more than two phases. Examining the contents of Table 4, recent publications include adaptations of TSFs [15, 24], DTC [25], model predictive control [26] or hysteresis control [27]. Refs. [15, 24] demonstrate the full speed range capability of their control schemes where ref. [24] reduces TR compared to other DTCs and ref. [15] lowers TR greatly. The other schemes do not present results at SRM rated speed. This does not mean that the control cannot function at this speed and all schemes do reduce TR comparatively to similar methods but do not eliminate it. The main goal of the GA is the absolute minimisation of the RMS current across a given SRMs operational torque and speed range. Notably, the GA at peak power operates at lower than the machines rated RMS and peak current, at 92.8% and 91% respectively. The closest comparison in terms of a percentage of rated power is ref. [25] which exhibits 49.9% of rated RMS current and 60% peak current at 50% rated power. Ref. [15] presents operation of an improved TSF function above the machines rated power of 120.8% but does not provide the machine rated currents they use to provide a percentage usage for comparison.

Comparing the speed range from 0 to 1500 rpm to the absolute minimal RMS current achievable by the given SRM (11.129A), an increase in RMS current of only 1.16% (3.2% increase in Cu loss) is present from 0 to 1000 rpm (two-phase overlap) and a maximum increase of 4.3% (8.8% increase in Cu loss) occurs from 1100 to 1500 rpm (three-phase overlap). Figure 17 conveys the ZTR speed limit of the GA method with two-phase overlap, three-phase overlap and the machines rated speed. The introduction of three-phase overlap optimises the

speed range established in ref. [21] while maintaining a minimal increase in RMS current and is shown capable of operating above the machines rated speed if required. This design itself is not limited to the 8/6 SRM used in this research and is applicable firstly to any SRM limited to only two-phase overlap in its design, and any other SRM configuration that is capable of greater than two-phase overlap. While intentional three-phase overlap is presented in this text, the method could be extended for even greater periods of phase overlap if the configuration in question desired this for operation at higher speeds while maintaining ZTR. Revisiting the profiles shown in Figure 16, there is some correlation between the shape of the current profiles with speed in terms of a consistent advance of θ_{on} and delay of θ_{off} in order to maintain production of >90% of FLT in the regions of $42°$ to $52°$ (high Nm/A). A point of future investigation could be the transition of this method to some form of online control scheme based upon FEA LUT of Nm/A efficiency, where near optimal RMS currents can still be produced while maintaining ZTR.

5.3 | Electric vehicle applications

In an EV application, maximum vehicle speed may occur at more than three times the base speed. This means that with constant speed cruising, which requires torque proportional to speed squared, far less than FLT is required. Figure 18 shows that the ZTR speed limit increases significantly with reducing torques. Torque in excess of this cruising requirement is available for acceleration (non-steady state, where defining and quantifying TR is problematic), hill climbing, towing, etc.

EV motors are fluid cooled. The inner/outer walled cooling jacket and its internal flow controlling ribbing, help minimised radial force movement of the stator around the alignment position. Machine vibration and noise can be minimised.

TABLE 4 Performance comparison of recent SRM publications.

	GA	[23]	[24]	[25]	[26]	[27]
Control parameter	T	I	T, ψ	T	T	T
SRM config. used	8/6	12/8	8/6	12/8	12/8	8/6
Zero TR speed range	≥100%	≥100%	≥53%	≥50%	≥1000 rpm	≥100%
(% ω_{rated})	@<1% TR	@<56.6% TR	@<13.5% TR	@<18.7% TR	@<8.7% TR	@<9.5% TR
RMS current						
(% I_{rated})	92.8%	63.1%	49.9%	N/A	N/A	15.22 A
(% P_{rated})	100%	38.1%	50.4%			120.8%
Peak current						
(% $I_{pk\ rated}$)	91%	73.4%	60%	~19A	N/A	~34A
(% P_{rated})	100%	38.1%	50.4%	10.5%		120.8%
Online/Offline	Offline	Online	Online	Online	Online	Offline

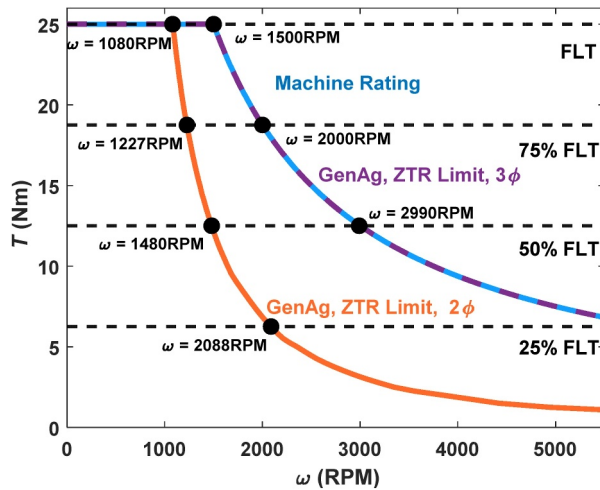Abbreviation: SRM, switched reluctance machine.

FIGURE 18 GA ZTR speed range and machine $T - \omega$ curve. GA, genetic algorithm; ZTR, zero torque ripple.

5.4 | Deployment on a control unit

When considering the application of the control scheme in common devices such as microcontrollers or field programmable gate arrays, the presented control scheme can be implemented in a relatively simple control architecture. With many offline control schemes, LUTs are typically implemented which provide data to be used as opposed to online calculations. With the proposed control scheme, implementation onto any control unit must consider the data storage requirements of the LUT itself. In an idealised control unit with large storage capabilities and extensive computational processing power, the GA LUT can be implemented with a high resolution in torque, speed and rotor position. This would be a large LUT and would provide the best performance, but practically an exchange must be made between resolution and storage. This is because in any given SRM, if there is insignificant resolution for any of the LUT variables, TR is likely to occur between interpolation points. This can either be resolved with the aforementioned sufficient resolution, where in this work a $15 - 4 - 601$ for speed, torque and angular resolution is used, or another possibility being the use of a lower resolution with some form of advanced interpolation utilised. Note that the main burden for high resolution required is in the angular step, which in the deployment of the scheme also means that a high resolution position sensor could also be required dependent on the resolution desired.

Another factor which should be considered for the practical application is certain effects which are not present in the FEA model utilised, which includes environmental effects such as temperature, which would likely account for a slight deviation in performance if not addressed given the difference that would be apparent between FEA and the real machine.

6 | CONCLUSION

This paper presented an offline refined GA design and control scheme for the elimination of TR and improving SRM efficiency across the entirety of an SRMs speed range. It

proposes the use of torque sharing beyond traditional two-phase torque sharing present in literature. It accomplishes this by using intentional three phase overlap as an example to allow the decay and build up of current without the introduction of increased TR as speed increases beyond the TR free speed limit of two phase torque sharing. The design itself produces current profiles at chosen speeds and torques while maintaining ZTR and utilising only the available DC link voltage provided. It also inherently minimises the RMS current of said profiles using the theoretically smallest RMS current available for the given SRMs configuration as a baseline to compare to. The results of the design are then converted into a LUT-based torque control scheme and validated through simulation using a detailed, FEA-based SRM model. A Comparison of the profiles are made with a standardly used TR elimination method, the Cosine TSF, is provided the GA control scheme is compared with recent publications on SRM control schemes. Overall the GA generates ZTR current profiles that result in less than 5% increased Cu losses above the theoretical minimum, over the full speed and torque range of an 8/6, 4 kW SRM while utilising the useful three-phase overlap.

AUTHOR CONTRIBUTIONS
Euan MacRae: Conceptualization; investigation; methodology; software; validation; writing—original draft. **Ali Abdel-Aziz**: Conceptualization; methodology; supervision; writing —review & editing. **Khaled Ahmed**: Funding acquisition; project administration; resources; supervision. **Richard Pollock**: Methodology; supervision. **Barry W. Williams**: Conceptualization; funding acquisition; methodology; project administration; writing—review & editing.

CONFLICT OF INTEREST STATEMENT
There are no conflicts of interest with this work.

DATA AVAILABILITY STATEMENT
The data that support the findings of this study are available on request from the corresponding author. The data are not publicly available due to privacy or ethical restrictions.

ORCID
Euan MacRae https://orcid.org/0009-0007-3765-2239
Khaled Ahmed https://orcid.org/0000-0002-7912-8140

REFERENCES
1. Gan, C., et al.: A review on machine topologies and control techniques for low-noise switched reluctance motors in electric vehicle applications. IEEE Access 6, 31430–31443 (2018). https://doi.org/10.1109/access.2018.2837111
2. Li, S., et al.: Modeling, design optimization, and applications of switched reluctance machines—a review. IEEE Trans. Ind. Appl. 55(3), 2660–2681 (2019). https://doi.org/10.1109/tia.2019.2897965
3. Zhu, Z.Q., Howe, D.: Electrical machines and drives for electric, hybrid, and fuel cell vehicles. Proc. IEEE 95(4), 746–765 (2007). https://doi.org/10.1109/jproc.2006.892482

4. Bilgin, B., et al.: Making the case for switched reluctance motors for propulsion applications. IEEE Trans. Veh. Technol. 69(7), 7172–7186 (2020). https://doi.org/10.1109/tvt.2020.2993725

5. Yang, Z., et al.: Comparative study of interior permanent magnet, induction, and switched reluctance motor drives for EV and HEV applications. IEEE Trans. Transp. Electrif. 1(3), 245–254 (2015). https://doi.org/10.1109/tte.2015.2470092

6. Lee, D.-H., Pham, T.H., Ahn, J.-W.: Design and operation characteristics of four-two Pole high-speed SRM for torque ripple reduction. IEEE Trans. Ind. Electron. 60(9), 3637–3643 (2013). https://doi.org/10.1109/tie.2012.2208432

7. Bostanci, E., et al.: Opportunities and challenges of switched reluctance motor drives for electric propulsion: a comparative study. IEEE Trans. Transp. Electrif. 3(1), 58–75 (2017). https://doi.org/10.1109/tte.2017.2649883

8. Zhu, J., et al.: Design of a new enhanced torque in-wheel switched reluctance motor with divided teeth for electric vehicles. IEEE Trans. Magn. 53(11), 1–4 (2017). https://doi.org/10.1109/tmag.2017.2703849

9. Cheok, A., Fukuda, Y.: A new torque and flux control method for switched reluctance motor drives. IEEE Trans. Power Electron. 17(4), 543–557 (2002). https://doi.org/10.1109/tpel.2002.800968

10. Inderka, R.B., De Doncker, R.W.A.A.: DITC-direct instantaneous torque control of switched reluctance drives. IEEE Trans. Ind. Appl. 39(4), 1046–1051 (2003). https://doi.org/10.1109/tia.2003.814578

11. de Paula, M.V., Barros, T.A.d.S.: A sliding mode DITC cruise control for SRM with steepest descent minimum torque ripple point tracking. IEEE Trans. Ind. Electron. 69(1), 151–159 (2022). https://doi.org/10.1109/tie.2021.3050349

12. Sun, Q., Wu, J., Gan, C.: Optimized direct instantaneous torque control for SRMs with efficiency improvement. IEEE Trans. Ind. Electron. 68(3), 2072–2082 (2021). https://doi.org/10.1109/tie.2020.2975481

13. Schramm, D.S., Williams, B.W., Green, T.C.: Torque ripple reduction of switched reluctance motors by phase current optimal profiling. In: PESC '92 Record. 23rd Annual IEEE Power Electronics Specialists Conference June–July (1992). https://doi.org/10.1109/PESC.1992.254793

14. Vujičić, V.P.: Minimization of torque ripple and copper losses in switched reluctance drive. IEEE Trans. Power Electron. 27(1), 388–399 (2012). https://doi.org/10.1109/tpel.2011.2158447

15. Li, H., Bilgin, B., Emadi, A.: An improved torque sharing function for torque ripple reduction in switched reluctance machines. IEEE Trans. Power Electron. 34(2), 1635–1644 (2019). https://doi.org/10.1109/tpel.2018.2835773

16. Ye, J., Bilgin, B., Emadi, A.: An extended-speed low-ripple torque control of switched reluctance motor drives. IEEE Trans. Power Electron. 30(3), 1457–1470 (2015). https://doi.org/10.1109/tpel.2014.2316272

17. Mademlis, C., Kioskeridis, I.: Performance optimization in switched reluctance motor drives with online commutation angle control. IEEE Trans. Energy Convers. 18(3), 448–457 (Sept 2003). https://doi.org/10.1109/tec.2003.815854

18. Al-Amyal, F., Al Quraan, L., Szamel, L.: Torque sharing function optimization for extended speed range control in switched reluctance motor drive. In: 2020 IEEE 3rd International Conference and Workshop in Óbuda on Electrical and Power Engineering (CANDO-EPE), pp. 119–124 (2020). https://doi.org/10.1109/CANDO-EPE51100.2020.9337792

19. Abraham, R., Ashok, S.: Data-driven optimization of torque distribution function for torque ripple minimization of switched reluctance motor. In: 2020 International Conference for Emerging Technology (INCET), pp. 1–6 (2020). https://doi.org/10.1109/INCET49848.2020.9154044

20. Feng, L., et al.: Direct torque control with variable flux for an SRM based on hybrid optimization algorithm. IEEE Trans. Power Electron. 37(6), 6688–6697 (June 2022). https://doi.org/10.1109/tpel.2022.3145873

21. MacRae, E., et al.: Genetic algorithm based approach of SRM current profiling for torque control and minimal copper losses. In: 2023 IEEE International Electric Machines & Drives Conference (IEMDC), San Francisco, CA, USA, pp. 1–7 (2023). https://doi.org/10.1109/IEMDC55163.2023.10239015

22. Abdel-Aziz, A.A., et al.: A neutral-point diode-clamped converter with inherent voltage-boosting for a four-phase SRM drive. IEEE Trans. Ind. Electron. 67(7), 5313–5324 (2020). https://doi.org/10.1109/tie.2019.2931268

23. Dessouky, Y.G., Williams, B.W., Fletcher, J.E.: A novel power converter with voltage-boosting capacitors for a four-phase SRM drive. IEEE Trans. Ind. Electron. 45(5), 815–823 (1998). https://doi.org/10.1109/41.720339

24. Xia, Z., et al.: A new torque sharing function method for switched reluctance machines with lower current tracking error. IEEE Trans. Ind. Electron. 68(11), 10612–10622 (2021). https://doi.org/10.1109/tie.2020.3037987

25. Ronanki, D., et al.: Phase current reconstruction method with an improved direct torque control of SRM drive for electric transportation applications. IEEE Trans. Ind. Appl. 58(6), 7648–7657 (2022). https://doi.org/10.1109/tia.2022.3196329

26. Song, S., et al.: High-dynamic four-quadrant speed adjustment of switched reluctance machine with torque predictive control. IEEE Trans. Ind. Electron. 69(8), 7733–7743 (2022). https://doi.org/10.1109/tie.2021.3108707

27. Song, S., et al.: Torque ripple and efficiency online optimization of switched reluctance machine based on torque per ampere characteristics. IEEE Trans. Power Electron. 35(9), 9608–9616 (2020). https://doi.org/10.1109/tpel.2020.2974662